Smart Human Serum Albumin-Indocyanine Green Nanoparticles Generated by Programmed Assembly for Dual-Modal Imaging-Guided Cancer Synergistic Phototherapy

Zonghai Sheng,[†,§] Dehong Hu,[†,§] Mingbin Zheng,[†] Pengfei Zhao,[†] Huilong Liu,[‡] Duyang Gao,[†] Ping Gong,[†] Guanhui Gao,[†] Pengfei Zhang,[†] Yifan Ma,[*,†] and Lintao Cai[*,†]

[†]Guangdong Key Laboratory of Nanomedicine, CAS Key Laboratory of Health Informatics, Shenzhen Institutes of Advanced Technology, Chinese Academy of Sciences, Shenzhen 518055, PR China and [‡]Department of Oncology, General Hospital of Beijing Command, PLA, Beijing 100700, PR China. [§]Z. S. and D. H. contributed equally to this paper.

ABSTRACT Phototherapy, including photodynamic therapy (PDT) and photothermal therapy (PTT), is a light-activated local treatment modality that is under intensive preclinical and clinical investigations for cancer. To enhance the treatment efficiency of phototherapy and reduce the light-associated side effects, it is highly desirable to improve drug accumulation and precision guided phototherapy for efficient conversion of the absorbed light energy to reactive oxygen species (ROS) and local hyperthermia. In the present study, a programmed assembly strategy was developed for the preparation of human serum albumin (HSA)-indocyanine green (ICG) nanoparticles (HSA-ICG NPs) by intermolecular disulfide conjugations. This study indicated that HSA-ICG NPs had a high accumulation with tumor-to-normal tissue ratio of 36.12 ± 5.12 at 24 h and a long-term retention with more than 7 days in 4T1 tumor-bearing mice, where the tumor and its margin, normal tissue were clearly identified *via* ICG-based *in vivo* near-infrared (NIR) fluorescence and photoacoustic dual-modal imaging and spectrum-resolved technology. Meanwhile, HSA-ICG NPs efficiently induced ROS and local hyperthermia simultaneously for synergetic PDT/PTT treatments under a single NIR laser irradiation. After an intravenous injection of HSA-ICG NPs followed by imaging-guided precision phototherapy (808 nm, 0.8 W/cm^2 for 5 min), the tumor was completely suppressed, no tumor recurrence and treatments-induced toxicity were observed. The results suggest that HSA-ICG NPs generated by programmed assembly as smart theranostic nanoplatforms are highly potential for imaging-guided cancer phototherapy with PDT/PTT synergistic effects.

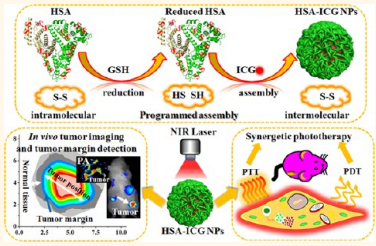

KEYWORDS: indocyanine green · theranostics · photothermal therapy · photodynamic therapy · synergistic effect · photoacoustic imaging

Phototherapy, represented by photodynamic therapy (PDT) and photothermal therapy (PTT), is a noninvasive and effective approach for cancer treatment.[1,2] This type of light-triggered treatment modality has remarkably improved selectivity and fewer side effects as compared to conventional radiotherapies and chemotherapies.[3] In phototherapy, light is administered, absorbed by the photosensitizer (PS) or photothermal agent, and converted into reactive oxygen species (ROS) or local hyperthermia, leading to tumor cell death.[4] To selectively and efficiently destroy the targeted cancer cells while sparing normal tissue, sufficiently enhancing the tumor accumulation of phototherapeutic agent, precisely focusing the laser beam on the tumor areas, and adequately converting the absorbed light energy to ROS or heat are important.[5−7] At present, several types of imaging technologies, including computed tomography (CT),[8] positron emission tomography (PET),[9] magnetic resonance imaging (MRI),[10−12] ultrasonic imaging[13] and photoacoustic imaging (PA)[14] have been applied as an assistance tool for guiding cancer phototherapy. However, real-time and precise control of the laser irradiation scope remain a major challenge as treatment required.[15] Thus, during laser treatment, it is necessary to real-time outline the tumor

* Address correspondence to lt.cai@siat.ac.cn, yf.ma@siat.ac.cn.

Received for review August 18, 2014 and accepted December 2, 2014.

Published online December 02, 2014
10.1021/nn5062386

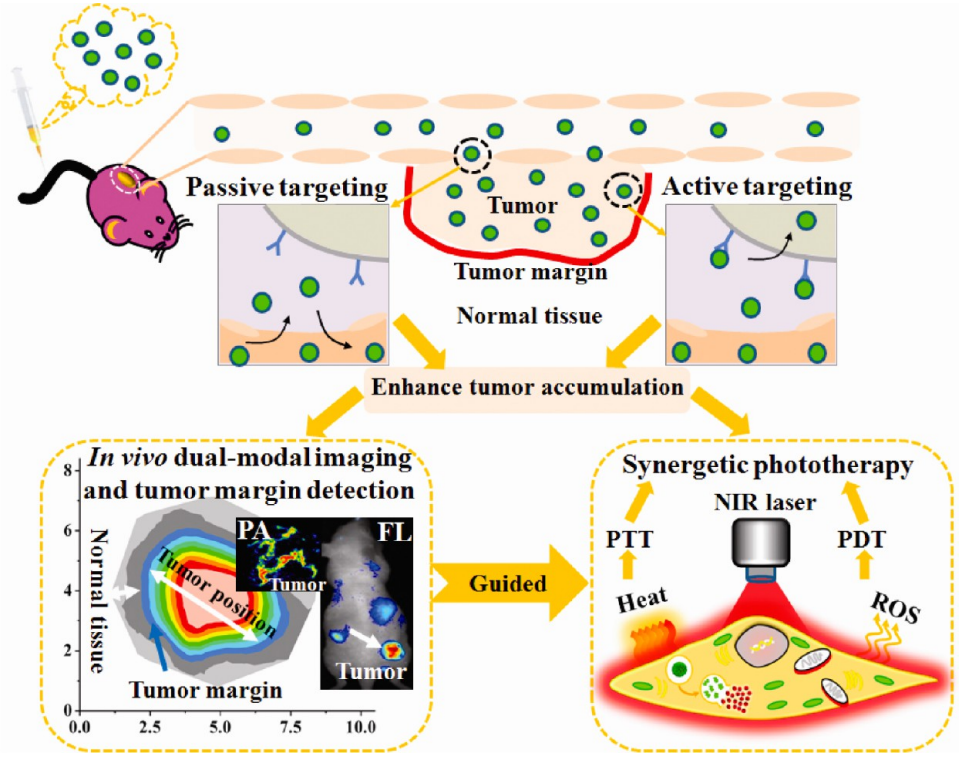

Figure 1. Schematic illustration of HSA-ICG NPs for *in vivo* dual-modal imaging, tumor margin detection, and simultaneous PDT/PTT treatments. Uptake of HSA-ICG NPs is presumably mediated by EPR effect (passive targeting) and the gp60 transcytosis pathway (active targeting) and subsequent binding to SPARC (secreted protein acidic and rich in cysteine, SPARC) in the tumor cells. The tumor, tumor margin and normal tissue could be detected using *in vivo* NIR and PA dual-modal imaging and spectrum-resolved technology. Upon the single NIR laser irradiation, the HSA-ICG NPs can simultaneously convert the absorbed light energy to ROS and heat for synergistic PDT/PTT treatments.

and its margin, normal tissue, which is prone to precisely focus the laser beam on the tumor areas. Fluorescence (FL) imaging in near-infrared (NIR) window (650−900 nm) holds much promise due to minimal autofluorescence and tissue scattering.[16] It not only could real-time monitor *in vivo* dynamic distribution of PS or photothermal agent, but also can detect the tumor and its margin, normal tissue using contrast enhancement and spectrum-resolved technology.[17] In addition, photoacoustic (PA) imaging has a high spatial resolution of optical imaging with the high penetration depth of ultrasound imaging, which can overcome some limits of NIR FL imaging.[18] Therefore, *in vivo* NIR FL and PA dual-modal imaging combined with spectrum-resolved technology would provide a real-time, sensitive, noninvasive assistant tool for cancer phototherapy.

In addition, to enhance the treatment efficiency and fully exert the synergistic effect of PDT and PTT, the PS and photothermal agent need to be simultaneously delivered to tumor in a site-specific manner.[19−22] Recent studies mainly focused on the PS-photothermal agent composite nanostructures for simultaneous PDT/PTT therapy triggered by a single NIR laser.[23,24] For instance, Wang *et al.* prepared photosensitizer-conjugated gold nanostars which could be induced both PDT and PTT effects by single wavelength NIR laser, and obtaining improved cancer therapy efficacy in MDA-MB-435 tumor bearing mice.[23] Lin *et al.* confirmed that photosensitizer-loaded plasmonic vesicular assemblies of gold nanoparticles (NPs) simultaneously excited by 671 nm laser for PDT/PTT treatments, which subsequently could significantly reduce tumor growth *in vivo*.[24] The unique treatment improved the therapeutic efficacy, reduced operation steps and time. However, the simultaneous synergistic therapy strongly depended on the overlapped both optical absorption of PS and photothermal agent. The particular requirement and complicated synthesis process could limit its further applications.

Indocyanine green (ICG) is a NIR dye for clinic approved by the U.S. Food and Drug Administration (FDA). It not only can be used for NIR FL and PA imaging, but also can convert the absorbed light energy to ROS and local hyperthermia for PDT and PTT, respectively.[25] Therefore, ICG could be considered as a kind of ideal theranostic platform for biomedical applications. Recently, several research groups including ours have developed some exogenous nanocarriers, such as polyallylamine,[26] calcium phosphosilicate,[27−29] lipid−polymer,[30−33] and perfluorocarbon,[34−37] to prepare ICG NPs for improving stability and tumor-specificity. However, the tumor could be partially inhibited by the single photothermal or

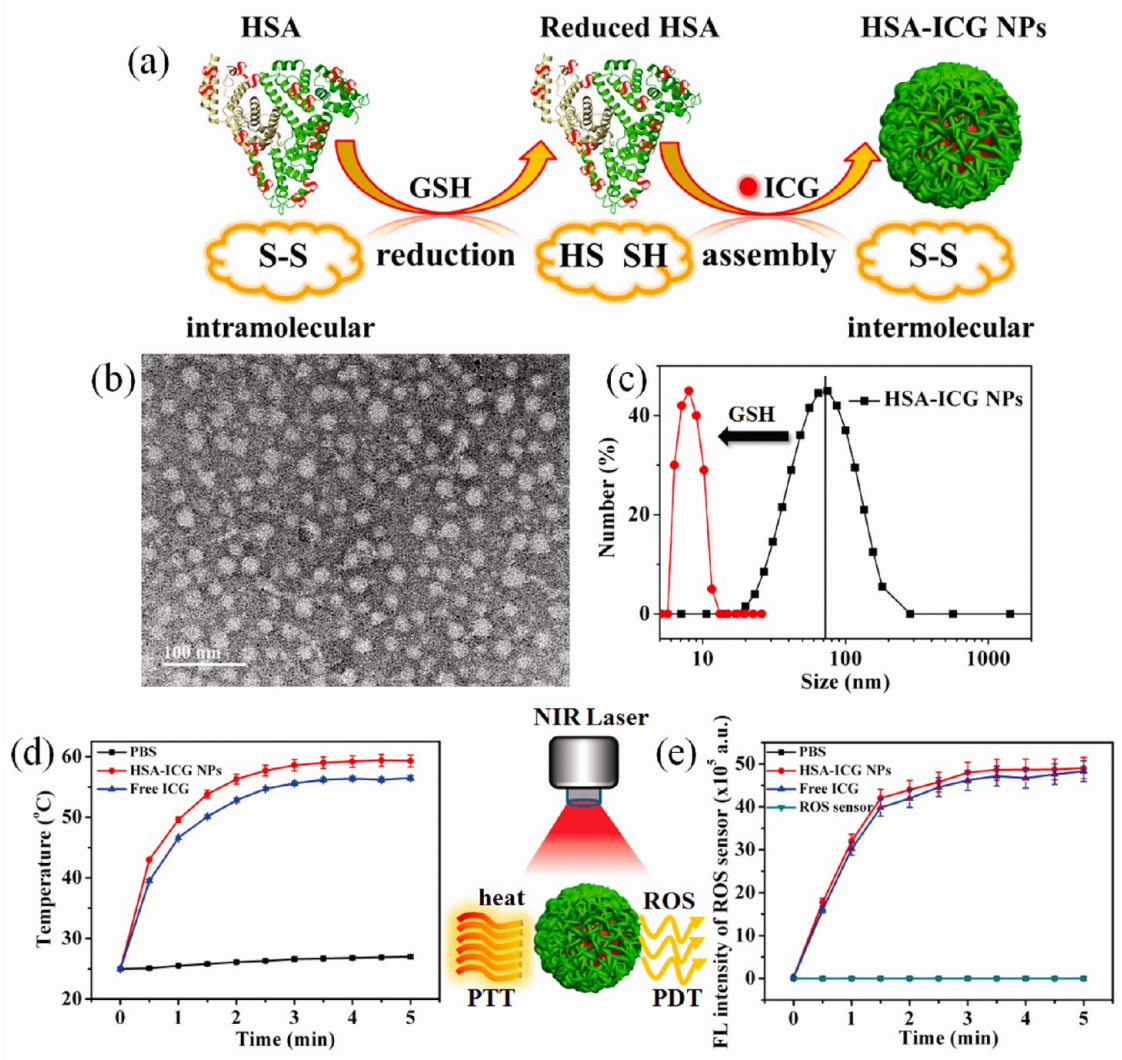

Figure 2. The synthesis and characterization of HSA-ICG NPs. (a) Schematic illustration of the programmed assembly strategy for the preparation of HSA-ICG NPs. (b) TEM image of HSA-ICG NPs, which were negatively stained with 2% phosphotungstic acid. (c) Size distribution of HSA-ICG NPs. (d) Time-dependent temperature and (e) singlet oxygen generation of HSA-ICG NPs during single NIR laser irradiation (808 nm laser, light dose rate: 1.0 W/cm^2), C_{ICG} = 0.2 mg/mL.

photodynamic effect of ICG.[29,31] Herein, a programmed assembly strategy was developed for fabricating ICG NPs using endogenous human serum albumin (HSA) as delivery system, applied for *in vivo* NIR FL and PA dual-modal imaging, tumor margin detection and simultaneous synergistic PDT/PTT therapy (Figure 1). The tumor could be completely ablated, and on tumor recurrence was observed. The smart HSA-ICG NPs have some unique advantages. (1) Biosafety: as an endogenous protein approved by FDA for intravenous administration, HSA as ICG delivery system is nontoxic, nonantigenic, and biodegradable.[38,39] (2) Tumour targeting: HSA NPs possess both passive and active tumor-targeting abilities *via* enhanced permeability and retention (EPR) effect and gp60 and SPARC receptor-mediated transcytosis, respectively.[40] (3) Stimuli response: HSA NPs are prepared with intermolecular cross-linking by disulfide bond, which exhibit excellent reductive-sensitive activity.[41] (4) Theranostics: HSA-ICG NPs can be used for tumor imaging and its margin detection, and synergistic PDT/PTT treatments.[25]

RESULTS AND DISCUSSION

Synthesis and Characterization of the HSA-ICG NPs. HSA is the most abundant plasma protein. Each HSA molecular is composed of one sulfhydryl group and 17 pair of disulfide bonds.[39] In this study, the HSA was incubated with excessive glutathione (GSH), an endogenous reducing agent, and these disulfide bonds of HSA molecular were cleaved. The obtained free sulfhydryl groups were assembled again by intermolecular disulfide bonds and formed HSA NPs (Figure 2a). No exogenous cross-linkers and toxic chemicals were involved during the preparation process. To verify our hypothesis, the changes of the total number of sulfhydryl group of HSA were first monitored with Ellman's method.[42] As HSA was incubated with excessive GSH, the average number of free sulfhydryl in each

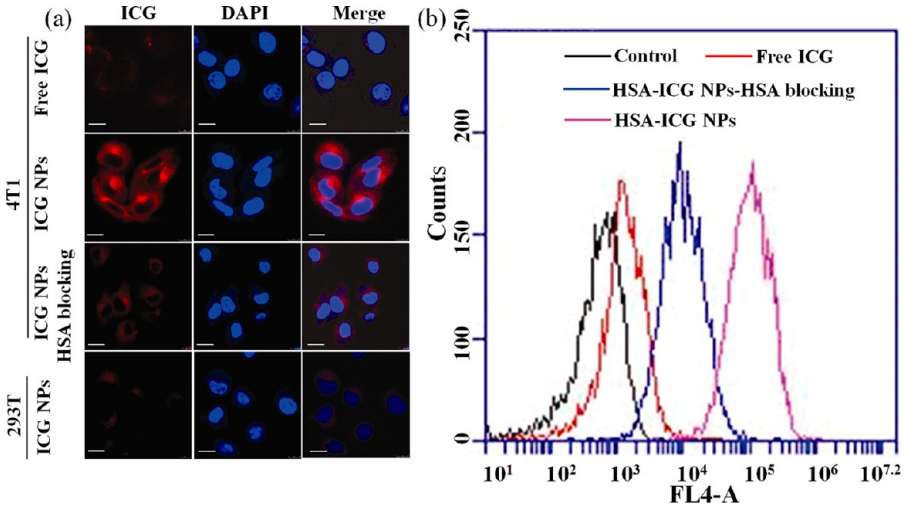

Figure 3. Cell uptake of free ICG and HSA-ICG NPs. (a) Confocal FL images of 4T1 and 293T subcellular localization of free ICG and HSA-ICG NPs after 3 h incubation. Blue represented FL of DAPI, and red represented FL of ICG. (b) Flow cytometric analysis of mean FL intensity (n = 10 000 cells) in 4T1 cells incubated with media (black), free ICG (red), HSA-ICG NPs with HSA blocking (blue) and HSA-ICG NPs (purple) for 3 h.

HSA molecular increased from 0.45 to 4.6, then decreased to 0.5 after formation of HSA-ICG NPs (Figure S1, Supporting Information). These varies of the number of sulfhydryl group indicated the formation process of intermolecular disulfide bonds, which are prone to stabilize the HSA-ICG NPs and make the NPs have reductive-sensitive activity. The circular dichroism (CD) spectra analysis was conducted to examine the characteristic of HSA's secondary structures (Figure S2). The results illustrated that the absorbance of HSA NPs in the range from 190 to 255 nm was almost same as natural HSA, indicating that the secondary structuring of HSA, including α helix, β sheet and random coil, did not change during the whole process.[43]

The size of HSA-ICG NPs could be turned by changing the amount of ethanol (Figure S3). Considering the size distribution and ICG loading efficiency, the optimized assembly approach was used in following experiments. As shown in Figure 2b, the obtained HSA-ICG NPs dispersed as individual NPs with a well-defined spherical shape and homogeneously distributed with diameter ranging from 25 to 35 nm. The average hydrodynamic diameter of HSA-ICG NPs was 75 $\pm$ 2.4 nm *via* DLS measurement (Figure 2c), which was larger than corresponding TEM results. The reason was that DLS showed an average hydrodynamic particle size, while TEM images detected the dehydration morphology of HSA-ICG NPs. When GSH (50 mM) was added into HSA-ICG NPs, the average hydrodynamic size of HSA-ICG NPs was decreased to 8.0 $\pm$ 0.6 nm, which indicated that prepared HSA-ICG NPs had excellent reductive-sensitive activity (Figure 2c). The zeta potential of HSA-ICG NPs was -39.0 ± 0.7 mV (Figure S4). The content of ICG in HSA NPs was 11.0% determined by UV/vis absorption spectra. The encapsulation of ICG in HSA NPs prevented its interaction with the surrounding environment and delayed its decomposition thus improving the photothermal and colloid stability and biocompatibility of ICG (Figure S5−S7). Upon the NIR laser irradiation, the temperature of HSA-ICG NPs increased to 59.4 °C, while the PBS only increased to 26.9 °C (Figure 2d). The results suggested that HSA-ICG NPs could cause significant hyperthermia, leading to an irreversible damage to tumor cells (above 42 °C).[2] The process for photothermal response of HSA-ICG NPs was accompanied simultaneously by generation of ROS. As showing Figure 2e, the FL intensity of singlet oxygen sensor (2′,7′-dichlorofluorescin diacetate, Figure S8) generation from HSA-ICG NPs increased with prolonging the laser irradiation time, indicating continuous generation of singlet oxygen by HSA-ICG NPs. The above results indicated that HSA-ICG NPs could be used as a photothermal and photodynamic agent for simultaneous PDT/PTT therapy triggered by single NIR laser. Moreover, the generation of singlet oxygen of HSA-ICG NPs enhanced with temperature rise (Figure S9). The result exhibited the photothermal effect mediated by HSA-ICG NPs was benefit for PDT enhancement.[44] Therefore, the simultaneous synergistic PDT/PTT effect induced by HSA-ICG NPs with single NIR laser could adequately convert the NIR laser energy to ROS and local hyperthermia for enhanced phototherapy.

***In Vitro* Cell Uptake and Synergistic Phototherapy.** The cell uptake behavior of free ICG and HSA-ICG NPs was investigated through confocal microscopy (Figure 3a). After 3 h incubation, a little amount of free ICG was observed in 4T1 breast cancer cells. In contrast, a large number of HSA-ICG NPs entered into cancer cells and localized in the cytoplasm. On the contrary, when the HSA-ICG NPs incubated with normal cells (293T human kidney cells) under the same conditions, low FL signal

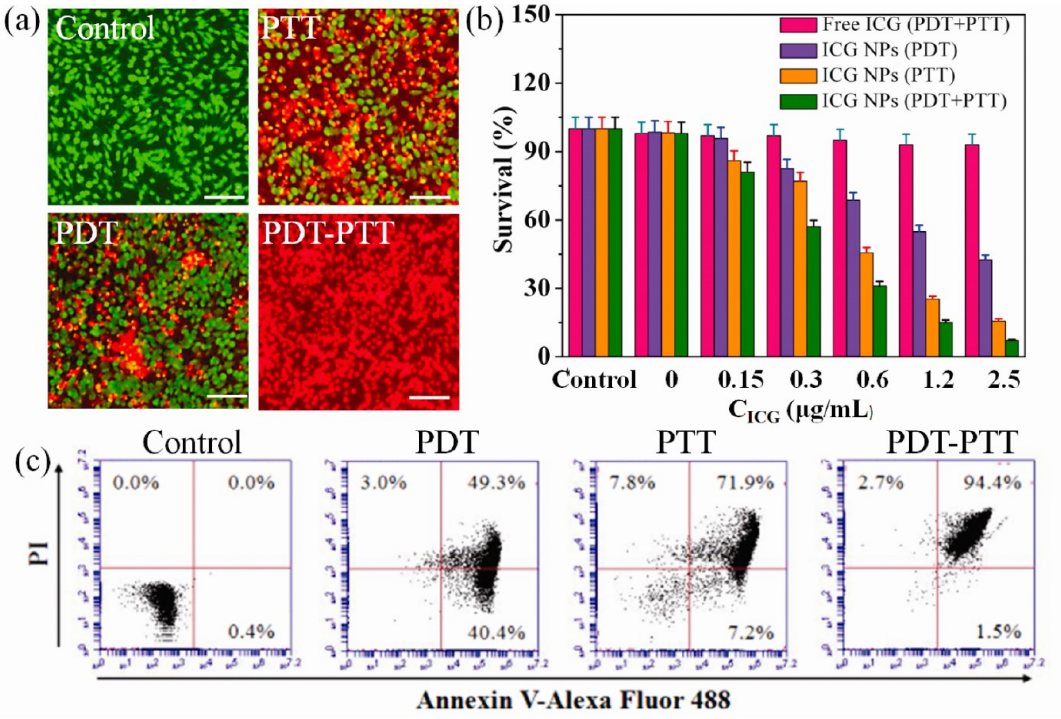

Figure 4. ***In vitro*** **phototherapy. (a) FL image of 4T1 cells after PDT, PTT and simultaneous PDT/PTT treatments. Viable cells were stained green with calcein-AM, and dead/later apoptosis cells were floating and eluted, or stained red with PI, C_{ICG} = 2.5 μg/mL. (b) Quantitative detection of 4T1 cells viability following PDT, PTT and simultaneous PDT/PTT treatments for 3 h. The date are shown as mean $\pm$ SD (n = 3). (c) Flow cytometry analysis of 4T1 cells after PDT, PTT and simultaneous PDT/PTT treatments. Positive PI and Annexin V-Alexa Fluor 488 cells were defined as late apoptosis/necrotic cells. C_{ICG} = 2.5 μg/mL.**

was observed in the cytoplasm (Figure 3a). To further demonstrate the active tumor-targeting ability of HSA-ICG NPs, the competition binding experiments using HSA were performed. A large number of HSA-ICG NPs entered into 4T1 cancer cells compared to the HSA-ICG NPs with blocking group (Figure 3a). The quantitative results of flow cytometric analysis showed that the average FL intensity was 10.3-fold greater in HSA-ICG NPs group than that in HSA-ICG NPs with HSA blocking group (Figure 3b). The results demonstrated that the encapsulation of ICG in HSA NPs could improve cell uptake ability, and enhance cancer cell targeting. The reasons probably were due to the presence of albumin receptor, SPARC (Secreted Protein, Acidic and Rich in Cysteine), in 4T1 cells. HSA-binding with SPARC and subsequent uptake by tumor cells increased its accumulation in cancer cells.[39] The enhanced cell uptake of HSA-ICG NPs was beneficial for improving the phototherapeutic efficiency.

Under the NIR laser irradiation, the HSA-ICG NPs in cancer cells could induce ROS and local hyperthermia generation, which can be detected using DHE probe and an infrared thermal camera, respectively (Figure S10−S11). In order to visually evaluate the *in vitro* therapeutic effect of HSA-ICG NPs, the cells were stained with calcein-AM and propidium iodide (PI) to identify live and dead/late apoptotic cells, respectively. As shown in Figure 4a, cells all displayed green FL in the control group, which suggested that pure laser irradiation alone cannot kill cells. To achieve single PDT and PTT treatments, we maintained a constant temperature (25 °C) or treated cells with 100 mM NaN_3, a well-known $^1O_2$ scavenger, in order to avoid producing singlet oxygen during laser irradiation.[21] These results illustrated that some cells were killed and exhibited red FL in the single PDT and PTT treated groups. On the contrary, without any post-treatments, HSA-ICG NPs provided simultaneously synergetic PDT/PTT to induce most of cells death and exhibiting intense homogeneous red FL. The quantitative treatment effect of HSA-ICG NPs was examined by MTT assay on 4T1 cells. As shown in Figure 4b, single PDT and PTT caused 57.5 and 84.4% of cell dead, respectively. The simultaneous PDT/PTT treatments further induced cell death up to 92.8%. The results were further validated by flow cytometry (Figure 4c). The 4T1 cells were treated with PDT, PTT, and simultaneous PDT/PTT, then labeled with PI and Annexin V-Alexa Fluor 488, respectively. The results showed that simultaneous PDT/PTT treatment more significantly induced 4T1 cell late apoptosis/necrosis (94.4%) as compared with single PDT (49.3%) or PTT (71.9%). It suggested that the simultaneous synergistic PDT/PTT effect was responsible for the improved therapeutic efficiency of HSA-ICG NPs.

In Vivo **Dual-Modal Imaging and Tumour Margin Detection.** The feasibility of HSA-ICG NPs for *in vivo* NIR FL and PA dual-modal imaging and tumor margin detection was investigated. Athymic nude mice with subcutaneous

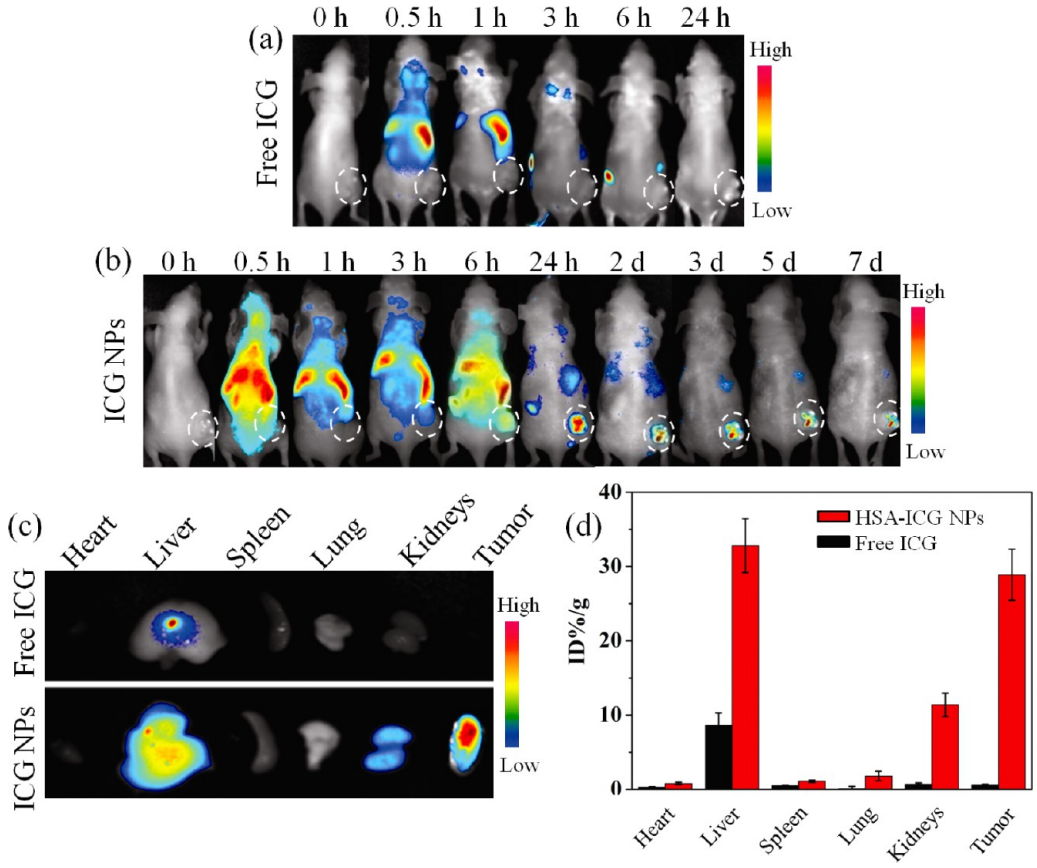

Figure 5. ***In vivo*** **FL imaging of nude mice bearing 4T1 tumors after i.v. injection of free ICG and HSA-ICG NPs, respectively. *In vivo* FL imaging results of (a) free ICG and (b) HSA-ICG NPs at different time intervals. (c) *Ex vivo* FL images of major organs and tumors after injection of free ICG and HSA-ICG NPs at 24 h. (d) Biodistribution of free ICG and HSA-ICG NPs in mice determined by the ICG FL from diluted tissue lysates. The data are shown as mean ± SD (n = 3).**

4T1 breast cancer xenografts were used as the animal modal. When the size of tumors reached ~60 mm^3, the mice were intravenously injected with free ICG and HSA-ICG NPs, respectively, and acquired FL images on CRI maestro system using a 704 nm excitation wavelength and a 735 nm filter at different time points. As shown in Figure 5a, in the case of free ICG-treated mice, the FL signals distributed extensively in liver tissue and less in tumor tissue after 0.5 h postinjection, and completely disappeared after 24 h postinjection. On the contrary, the FL signal of tumor tissue strengthened with the increase of time interval, and reached a peak after 24 h postinjection of HSA-ICG NPs (Figure 5b). After 7 days, the FL signal in tumor tissue still could be detected. The pharmacokinetic data showed that the blood circulation half-life of HSA-ICG NPs was significantly prolonged compared to free ICG ($t_{1/2}$ HSA-ICG NPs =2.86 h *vs* $t_{1/2}$ free ICG =0.12 h), indicating the long blood circulation time of HSA-ICG NPs (Figure S12). The *ex vivo* images of major organs and tumors demonstrated that most of ICG accumulated in the liver 24 h after i.v. injection of free ICG. The HSA NPs dramatically increased the accumulation of ICG in tumor, followed by liver and kidneys (Figure 5c). The HSA-ICG NPs biodistribution in various tissues was detected, and expressed as percentage of dose per unit mass of tissue (% ID/g). As shown in Figure 5d, at 24 h postinjection, the ICG content in tumor reaches maximum of about 28.8% dose/g tissue, and tumor-to-normal tissue ratio is 36.12 ± 5.12, suggesting high tumor accumulation ratio.

As a dual-modal contrast agent, the HSA-ICG NPs exhibited an excellent property of PA imaging (Figure S13). As showing Figure 6a, before i.v. injection of free ICG and HSA-ICG NPs, only large blood vessels in tumor could be visualized using hemoglobin as an endogenous contrast agent.[4] After i.v. injection of free ICG and HSA-ICG NPs, the PA signals at tumor tissue increased over time (Figure 6b). The HSA-ICG NPs exhibited stronger PA signal than that of free ICG, which agreed with the *in vivo* NIR FL imaging behavior. The enhanced PA signals after 24 h postinjection visually revealed the uniform distribution of ICG within and outside the tumor microvessels. The results showed that HSA-ICG NPs-based PA imaging provided a high spatial resolution, which is prone to understand the distribution of ICG in tumor tissue and get the information on tumor microstructure.

The real-time, sensitive and long-term NIR FL and PA dual-modal imaging is useful in confirming tumor

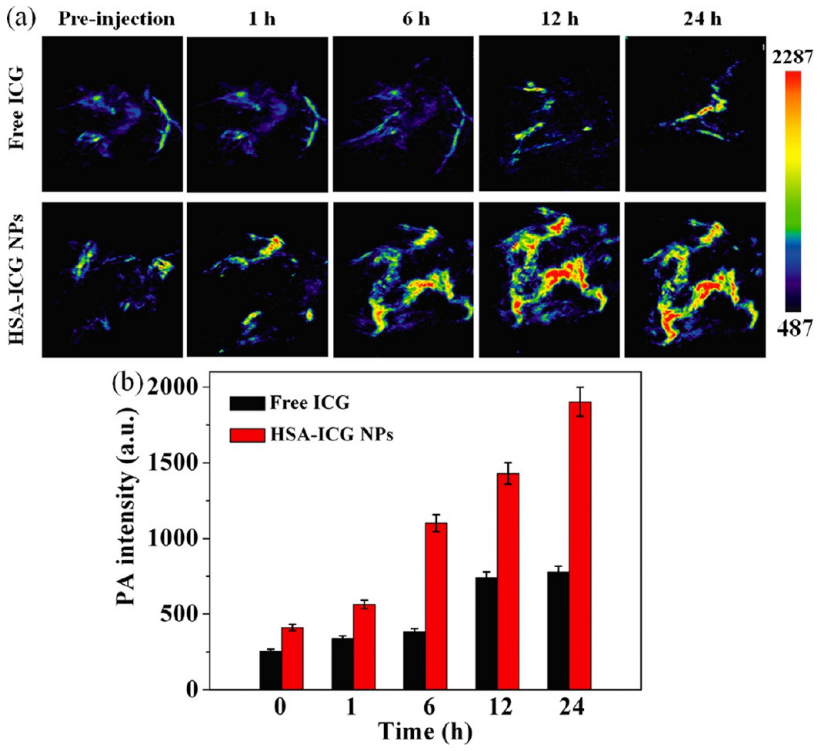

Figure 6. *In vivo* tumor PA imaging. (a) PA imaging of the mice bearing 4T1 tumor injected with free ICG and HSA-ICG NPs at different times. (b) The mean PA intensity of tumor tissue at 0, 1, 6, 12, and 24 h postinjection, respectively. The data are shown as mean ± SD (n = 3).

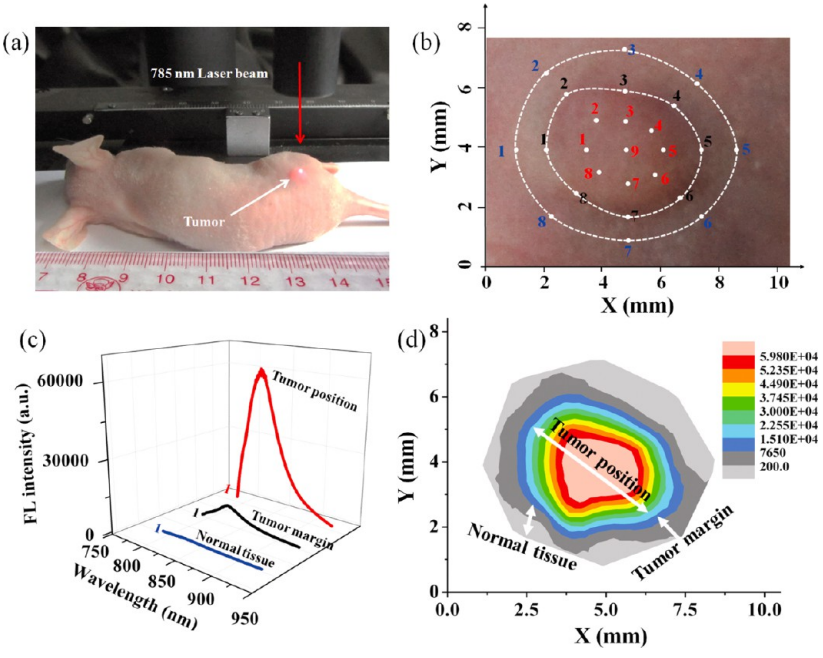

Figure 7. *In vivo* tumor margin detection. (a) Photograph showing a laser beam focusing on the tumor site. *In vivo* FL spectra were obtained from the tumor site, tumor margin, and normal tissue at 785 nm excitation. (b) Photograph of tumor, tumor margin and normal tissue labeled with different numbers. (c) Averaged FL spectra of the tumor site, tumor margin and normal tissue. (d) Tumour mapping imaging with integrated FL intensity of HSA-ICG NPs at various locations.

location, detecting tumor large blood vessels and optimizing the content of phototherapeutic agents.[14] However, scattering of light in tumor tissue severely impedes imaging of tumor margin.[15] Therefore, it is essential to identify the tumor margin for planning spatially localized phototherapy. For proof-of-concept, ICG-based FL spectrum-resolved technology provided a promising tool for highly sensitive detection of tumor boundary.[17] 785 nm NIR laser was carried out as an excitation wavelength, and the *in vivo* emission

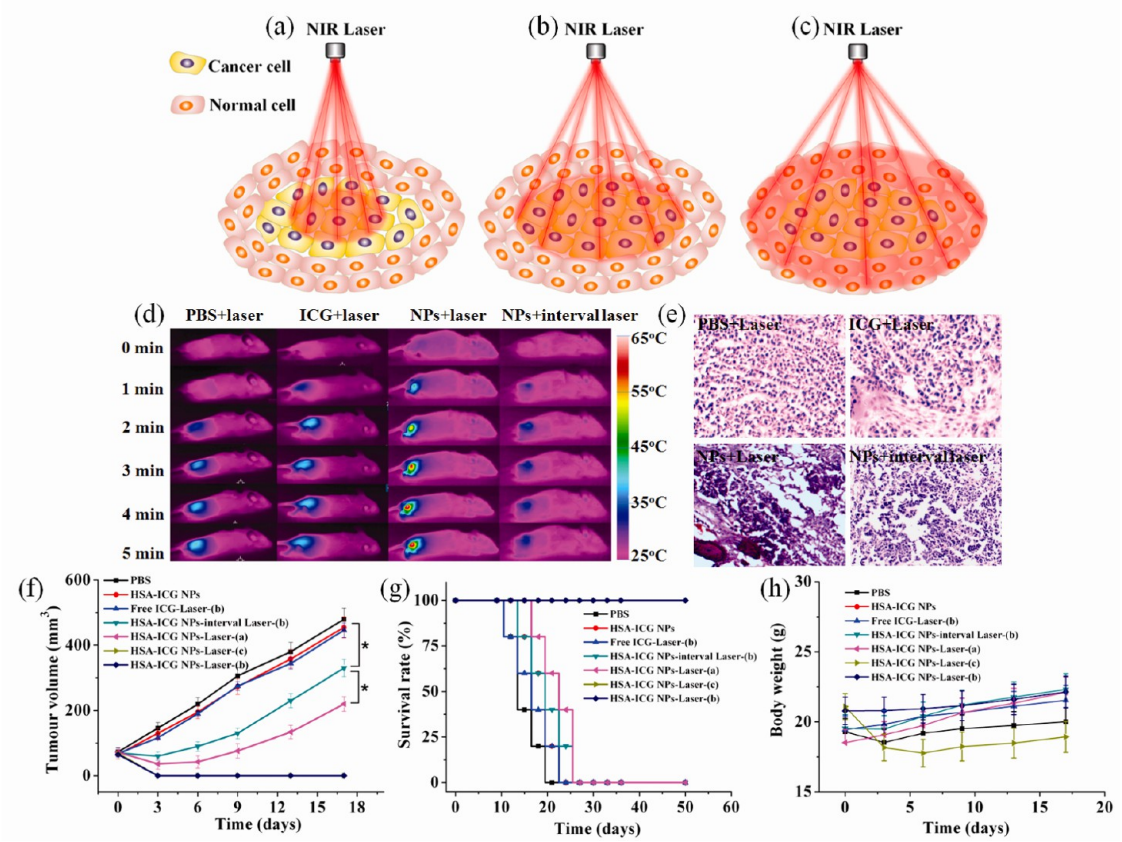

Figure 8. *In vivo* **cancer phototherapy in xenograft mice models with 4T1 breast cancer. Schematic illustration shows the tumor tissue was irradiated by NIR laser beam with three different ways: (a) part irradiation, (b) accurate irradiation, (c) over irradiation. (d) IR thermal images of 4T1 tumor-bearing mice exposed to 808 nm laser for 5 min (0.8 W/cm^2). (e) H&E stained images of tumor sections collected from different treated groups of mice 4 h post treatment. (f) Tumour growth curves of different groups of 4T1 tumor-bearing mice. (g) Survival rates of mice bearing 4T1 tumors after different treatments. (*)$p < 0.05$, (**)$p < 0.01$. (h) Body weights were measured during the 17 day evaluation period in mice under the different conditions. Dates indicate means and standard errors.**

spectrum of HSA-ICG NPs was obtained with spectrometer (Figure 7a). As shown in Figure 7b, the tumor and its margin, normal tissue sites were first labeled with different color numbers. We detected the FL spectra of ICG at normal tissue, tumor margin and tumor position using spectrum-resolved technology (Figure 7c). The ICG exhibited a characteristic emission spectra with the peak located at 816 nm. The average FL intensity of tumor positions is nearly 270 times than that of normal tissue. The FL intensity collected from the tumor margin (less than 1 mm from tumor) are still 19 times stronger than that of normal tissue, providing excellent delineation of the tumor. Integrated FL intensity of ICG at various locations was translated into a mapping imaging using origin software (Figure 7d). The results were indeed correlated with presence of tumor and its margin, normal tissue as determined with bright-field image. Therefore, *in vivo* NIR FL imaging and HSA-ICG-based spectrum-resolved technology can precisely identifying tumor position, size and margin, which are prone to guide focusing laser beam on whole tumor tissue without damaging normal tissue.

Imaging-Guided *In Vivo* Synergistic Phototherapy. On the basis of the treatment results *in vitro*, we expected to apply HSA-ICG NPs for *in vivo* cancer phototherapy. Under the guidance of NIR FL and PA dual-modal imaging and spectrum-resolved technology, the laser beam could be manipulated very precisely and flexibly, and accurately focused on the whole tumor tissue (Figure 8b). The real-time temperature change of mice was analyzed using an infrared thermal camera, which provided an effective tool for monitoring the treatment process. As shown in Figure 8d, after the 5 min of NIR laser irradiation, the tumors treated with PBS and free ICG exhibited moderate increase to 37.8 and 40.6 °C, respectively. While the temperature of tumor treated with HSA-ICG NPs increased rapidly to 57.2 °C, which was high enough to ablate the malignant cells. In order to confirm the PDT effect *in vivo*, the laser irradiation was adjusted using the 5 min interval after each minute of irradiation. The tumor exhibited a mild temperature rise to 32.4 °C, which was insufficient to irreversibly heat damage the tumor tissue. To determine the antitumor effect of free ICG and HSA-ICG NPs mediated by heat or ROS, H&E staining of tumor

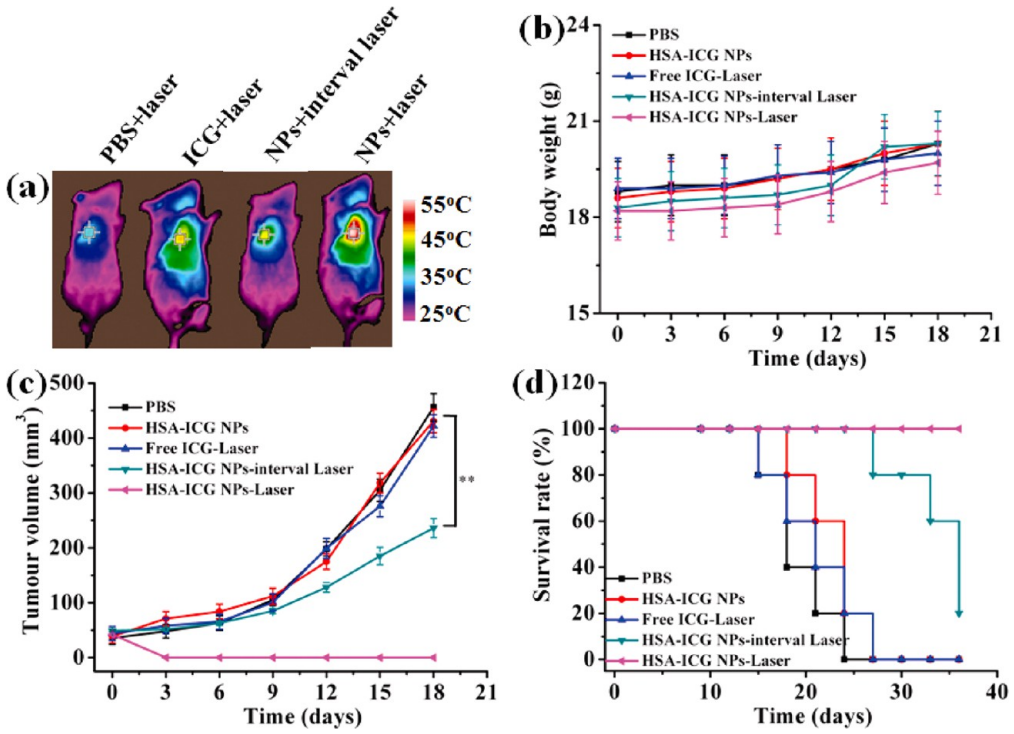

Figure 9. *In vivo* **cancer phototherapy in orthotopic mice models with 4T1 breast cancer. (a) IR thermal images of 4T1 tumor-bearing mice exposed to 808 nm laser for 5 min (0.8 W/cm^2). (b) Body weights were measured during the 18 day evaluation period in mice under the different conditions. Dates indicate means and standard errors. (c) Tumour growth curves of different groups of 4T1 orthotopic mice. (d) Survival rates of orthotopic mice bearing 4T1 tumors after different treatments. (*)$p < 0.05$, (**)$p < 0.01$.**

sections was performed. As shown in Figure 8e, in PBS and free ICG treated groups, there was no obvious tumor necrosis in histological section. On the contrary, abundant karyolysis and sporadic necrotic was observed in HSA-ICG NPs treated group with interval laser irradiation (PDT), and apparent extensive cancer necrosis occurred with continuous NIR laser irradiation (PDT/PTT). The results indicated that simultaneous PDT/PTT effect *in vivo* could be induced by single NIR laser irradiation. HSA-ICG NPs can coordinate PDT with PTT to get higher anticancer efficiency than single PDT therapy in living mice.[45]

In order to further investigate the antitumor efficiency of HSA-ICG NPs in mice bearing 4T1, the growth rate of tumors was monitored every 3 days after treatments (Figure 8f). The represent mice photos reflecting the tumor size change showed in Figure S14. The tumors treated with PBS and HSA-ICG NPs without laser irradiation and free ICG plus laser irradiation grew rapidly, indicating the 4T1 tumor growth was not affected by HSA-ICG NPs, free ICG or laser irradiation. The growth of 4T1 tumors was slightly inhibited by HSA-ICG NPs plus interval and laser irradiation, which indicated that the HSA-ICG NPs for PDT triggered by interval laser irradiation could partly suppress tumor growth, but tumor regrew after 3 days post-treatment. The survival rate of this group was 40.0% on day 20 post-treatment (Figure 8g). When the continuous NIR laser beam was accurately focused on the whole tumor tissue (Figure 8b), the growth of 4T1 tumor was completely inhibited with 100% of survival rate on day 50, and there was no tumor recurrence detected. The simultaneous synergetic PDT/PTT therapy mediated by HSA-ICG NPs plus single NIR laser could significantly improve the phototherapeutic efficiency. During the treatments, the body weight was monitored, which indicated the treatments-induced toxicity (Figure 8h). On day 17, the weight of the control groups treated with PBS and HSA-ICG NPs in mice bearing 4T1 gradually increased by 6 and 11%, and those treated with HSA-ICG NPs and free ICG plus continuous or interval laser increased by 7, 8 and 11%. These groups were not significantly different from the control group, suggesting that the treatment was reasonably well-tolerated. Moreover, the H&E staining images of major organs collected from HSA-ICG NPs treated groups with NIR laser showed that neither obvious damage nor inflammation was observed compared to the control group (Figure S15). The results indicated that the HSA-ICG NPs possessed low cytotoxicity, and being suitable for imaging-guided simultaneous synergistic PDT/PTT therapy.

On the other hand, the continuous NIR laser beam would be partly or over focused on the tumor tissue without imaging-guided technology (Figure 8a and 8c). In HSA-ICG NPs treated groups with partly laser beam irradiation, the growth of 4T1 tumor was partly inhibited, and regrow after 6 days post-treatment

(Figure 8f). The survival rate of this group was 60% on day 20 post-treatment (Figure 8g). On the contrary, when the NIR laser beam was over focused on the tumor position, the growth of 4T1 tumor was completely suppressed (Figure 8f). However, the body weight of the treated mice decreased rapidly by 23%, suggesting that the treatment has high side effects (Figure 8g). The results demonstrated that the imaging-guided phototherapy was prone to accurately focus the NIR laser beam on the tumor and improve the treatment efficiency and reduce treatments-induced toxicity.

On the basis of the encouraging results, the HSA-ICG NPs for synergistic phototherapy were further investigated in an orthotopic breast cancer model. The breast tumor grew on the mammary fat pad of mice, keeping a distance from the surface skin.[46] The mice were treated when the tumor reached 40 mm^3. The results were shown in Figure 9. After the NIR laser irradiation for 5 min, the tumors treated with HSA-ICG NPs exhibited high increase to 53.8 °C, which was high enough to ablate the malignant cells. The growth of 4T1 tumor in orthotopic mice models was completely inhibited with 100% of survival rate on day 18, and there was no tumor recurrence detected (Figure S16). The results indicated that the HSA-ICG NPs could also be successfully applied for tumor phototherapy in breast tumors in orthotopic mice models.

CONCLUSION

The present study reported a programmed assembly strategy to fabricate HSA-ICG NPs successfully for *in vivo* dual-modal imaging and tumor margin detection following PDT/PTT synergetic phototherapy. The advantages of the prepared method are as follows: (1) It could effectively maintain the biological activity of HSA without using exogenous cross-linkers and toxic chemicals; (2) The encapsulation of ICG in HSA NPs remarkably improved the stability of ICG; and (3) HSA NPs enhanced delivery of ICG into cancer cells. The tumor, tumor margin and normal tissue could be clearly detected using ICG-based *in vivo* FL and PA dual-modal imaging and spectrum-resolved technology, which was prone to avoid the effect of light scattering and precisely guide cancer phototherapy. The HSA-ICG NPs-mediated simultaneous synergetic PDT/PTT treatments significantly improved the anticancer effect, leading to superior tumor eradication without any regrowth. Therefore, this novel theraonstic nanoplatform can be a promising strategy for imaging-guided synergetic cancer phototherapy, and is expected to have a great potential in clinical translation.

MATERIALS AND METHODS

Materials. HSA was obtained from Beijing Biosynthesis Biotechnology CO., Ltd. ICG, NaN_3, GSH, 3-(4,5-dimethylthiazol-2-yl)-2,5-diphenyltetrazolium bromide (MTT), 4,6-diamidino-2-phenylindole (DAPI), and propidium iodide (PI) were purchased from Sigma-Aldrich. Calcein-AM and Alexa Fluor 488 Annexin V/Propidium Iodide (PI) Cell Apoptosis Kit were obtained from Invitrogen (USA). Phosphate-buffered saline (PBS, pH 7.4), fetal bovine serum (FBS), RMPI 1640, trypsin-EDTA and penicillin-streptomycin were purchased from Gibco Life Technologies (AG, Switzerland). Ethanol was obtained from Sinopharm Chemical Reagent Co., Ltd. (Shanghai, China). Amicon ultra-4 centrifugal filter with a molecular weight cutoff of 100 kDa was bought from Millipore (USA). All other chemicals used in this study were of analytical reagent grade and used without further purification. Superpure water (18.25 MΩ.cm, 25 °C) was used to prepare all solutions. BALB/c athymic nude mice and BALB/c mice were maintained under aseptic conditions in a small animal isolator. All food, water, bedding and cages were autoclaved before use.

Determination of the Number of the Free Sulfhydryl. The number of the free sulfhydryl of HSA, reduced HSA and HSA NPs was determined using the Ellman's method.[42] The preparation of reduced HSA and HSA NPs was as follows. HSA was dissolved in deionized water at concentration 40 mg/mL with 50 mM GSH at room temperature to break up the intramolecular disulfide bonds and expose free sulfhydryl groups. After 60 min, 2 mL of solution were taken out to dialyze (membrane cutoff MW: 12 KD) in deionized water at 4 °C for 24 h to get rid of the excessive GSH and probably its oxidized form GSSG. Then, 2 mL of the desolvating agent ethanol was added into another 2 mL of solution to supersaturate the HSA solution and precipitate the NPs. The suspension was kept under stirring at room temperature for 30 min. After that, the suspension was dialyzed (membrane cutoff MW: 12−14 KD) with deionized water at 4 °C for 24 h to remove ethanol and GSH.

HSA-ICG NPs Generated by Programmed Assembly. 80 mg HSA and 20 mg ICG were first dissolved in 2 mL deionized water with 50 mM GSH at 37 °C for 1 h. Then, 2 mL of the ethanol was added into the solution to precipitate the HSA-ICG NPs. The suspension was kept under stirring at room temperature for 30 min. After that, the suspension was dialyzed (membrane cutoff MW: 12−14 KD) with deionized water at 4 °C for 24 h to remove ethanol, free ICG and GSH. To determine ICG loading in HSA-ICG NPs, the HSA-ICG NPs solution was diluted in 5 mL of DMSO/H_2O (9:1, v/v) and sonicated for 30 min to extract ICG completely. ICG levels were determined by UV/vis absorption spectra. ICG loading was defined as ICG content (%, w/w) = (ICG weight in HSA-ICG NPs/total HSA-ICG NPs weight) × 100. All the measurements were performed in triplicate.

Characterization of HSA-ICG NPs. The freshly obtained HSA-ICG NPs suspension were transferred onto a 200 mesh copper grid coated with carbon, stained with 2% (w/v) phosphotungstic acid, dried at room temperature, then analyzed by TEM (FEI Tecnai G2 F20 S-Twin, USA). UV/vis absorption spectra were obtained with a PerkinElmer Lambda 25 UV/vis spectrophotometer. The PL spectra were obtained by a FL spectrometer (F900, Edinburgh Instruments Ltd.). Circular dichroism (CD) spectra were recorded on an Applied Photophysis Chirascan instrument at 25 °C. The size and zeta potential of the HSA-ICG NPs were measured by dynamic light scattering (DLS), using a Malvern Zeta Sizer (NanoZS). The samples have been thoroughly purified with centrifugal filters from Millipore (Centrifugal filter devices, 100 K) and dispersed in superpure water prior to the measurements. Given the sensitivity of the instrument, multiple runs (>3) were performed to avoid erroneous results.

Single Oxygen Detection. 2′,7′-dichlorofluorescin diacetate was employed to evaluate the singlet oxygen generation of HSA-ICG NPs. A certain of HSA-ICG NPs was mixed with 2′,7′-dichlorofluorescin diacetate (1 μM) in water containing 2% DMSO. The mixture solutions were irradiated with an NIR laser

(808 nm, 1 W/cm^2). The fluorescence was excited with a light resource of 494 nm wavelength.

Cell Culture. The human embryonic kidney cell line 293T and mouse breast cell line 4T1 were cultured in RMPI 1640 supplemented with 10% (v/v) fetal bovine serum, 1% (v/v) penicillin, and 1% (v/v) streptomycin. Cells were incubated in a humidified incubator at 37 °C with 5% CO_2.

***In Vitro* Cell Uptake.** For *in vitro* studies, 1×10^5 4T1 and 293T cells were seeded on a glass-bottomed culture dish, respectively. After 24 h, HSA-ICG NPs or free ICG was incubated with different cells for 3 h at 37 °C. To remove the unbound conjugates, the cells were washed three times for 10 min by using shaking incubation in Tris buffer and fixed with 3.7% formaldehyde solution (1 mL) and incubated at shaking incubation each for 20 min. The nuclear dye DAPI was used as a positive control to stain nuclei in the experiment. Images of cells were acquired using a Leica DMI6000 inverted microscope with a Leica TCS SP5 confocal scanning system.

For cellular uptake experiment, the cells (1×10^5 cells per well) were seeded in 6-well plates and incubated overnight, and then incubated with 0.01 mg/mL HSA-ICG NPs or free ICG. After incubation 3 h, cells were rinsed with PBS three times, tripsinized, and resuspended with medium. Afterward, the cells were collected by Accuir C6 flow cytometer using CFlow Plus software (BD, Ann Arbor, MI).

DHE Staining. ROS formation was monitored by fluorescence microscopy using dihydroethidium (DHE) as the indicator. Briefly, 1×10^5 4T1 and 293T cells were seeded on a glass-bottomed culture dish. After 24 h, HSA-ICG NPs was incubated with different cells for 3 h at 37 °C. After the cells were washed 3 times using PBS, 0.2 mL of DHE solution (5 μM, PBS) was added into the cells for 30 min at 37 °C. Afterward, the cells were rinsed again with PBS, and subsequently illuminated using an 808 nm laser with energy density of 1 W/cm^2 for 5 min. Then, the nuclear dye DAPI was used as a positive control to stain nuclei in the experiment. Images of cells were acquired using a Leica DMI6000 inverted microscope with a Leica TCS SP5 confocal scanning system.

***In Vitro* Phototherapy.** 4T1 cells (1×10^4 cells per well) were seeded in 96-well plates and incubated overnight at 37 °C in a humidified 5% CO_2 atmosphere. After being rinsed with PBS (pH 7.4), the cells were incubated with HSA-ICG NPs for 3 h at 37 °C under the same conditions. Afterward, the cells of experimental group were rinsed again with PBS and immersed in 200 μL of fresh culture medium, and subsequently illuminated using an 808 nm laser with energy density of 1 W/cm^2 for 5 min. The PDT effect of HSA-ICG NPs on 4T1 cells were further verified by maintaining a constant temperature to avoid photothermal effect, and the PTT effect of HSA-ICG NPs were further verified by treating 4T1 cells with 100 mM NaN_3 to avoid producing singlet oxygen during laser irradiation. The laser spot was adjusted to fully cover the area of each well. After illumination, cells were incubated for 12 h in a 5% CO_2, 95% air humidified incubator at 37 °C. Dark control group was kept under identical conditions as the experimental group except for illumination. The standard MTT assay was carried out to evaluate the cell viability.

The synergistic PDT/PTT effects of HSA-ICG NPs on 4T1 cells were further verified using Calcein AM and propidium iodide (PI) costaining. 4T1 cells (5×10^4 cells per well) were seeded in 6-well plates and incubated overnight at 37 °C in a humidified 5% CO_2 atmosphere. After being rinsed with PBS (pH 7.4), the cells were incubated with HSA-ICG NPs or free ICG for 3 h at 37 °C under the same conditions. Afterward, the cells of experimental group were rinsed again with PBS and immersed in 200 μL of fresh culture medium, and subsequently illuminated using an 808 nm laser with energy density of 1 W/cm^2 for 5 min. After another 4 h incubation cells were stained with calcein-AM for visualization of live cells and with PI for visualization of dead/late apoptotic cells, according to the manufacturer's suggested protocol (Invitrogen). Afterward, the cells of experimental group were rinsed again with PBS and were examined by eliminating the interference of background FL of ICG with biological inverted microscope (Olympus IX71, JPN).

Animal Model. Animals received care in accordance with the Guidance Suggestions for the Care and Use of Laboratory Animals. The procedures were approved by Shenzhen Institutes of Advanced Technology, Chinese Academy of Sciences Animal Care and Use Committee. Six-to-seven week old male BALB/c athymic nude mice and BALB/c mice were maintained under aseptic conditions in a small animal isolator and were housed in a group of five in standard cages with free access to food and water and a 12 h light/dark cycle. All animals acclimated to the animal facility for at least 7 days before experimentation. BALB/c mice subcutaneous tumor models were established by subcutaneous injection of 1×10^6 4T1 cells onto the hind legs of mice. BALB/c mice orthotopic tumor models were developed as follow. 0.05 mL of the cell suspension was injected into the mammary fat pad inferior to the nipple using a 28-gauge needle. The breast tumor grew on the mammary fat pad of mice, keeping a distance from the surface skin. All possible parameters that may cause social stress, like group size, type (treated and nontreated), *etc*., among the experimental animals were carefully monitored and avoided. Animals were observed daily for any behavioral abnormalities and weighed weekly.

Blood Circulation. To detect the blood circulation half-life of HSA-ICG NPs, the BALB/c mice were randomly divided into 10 groups (n = 3 per group). Each group of mice was i.v. injected with 100 μL of HSA-ICG NPs. The blood samples with ~100 μL were drawn from orbit of BALB/c mice postinjection of HSA-ICG NPs at different time points (0.1, 0.2, 0.3, 0.5, 1, 3, 6, 8, 12, 24 h). Each blood sample was dissolved in 900 μL of lysis buffer. The concentration of HSA-ICG NPs in the blood was determined by the FL spectrum of each solubilized blood sample using a FL spectrometer. A series of dilutions of free ICG were measured to obtain a standard calibration curve. Blank blood sample without HSA-ICG NPs injection was measured to determine the blood autofluorescence level, which was subtracted from the FL intensities of injected samples during the concentration calculation. The HSA-ICG NPs are presented as the percentage of injected dose per gram of tissue (% ID/g).

***In Vivo* Tumour Imaging and Tumour Margin Detection.** Athymic nude mice with subcutaneous 4T1 breast cancer xenografts were used as the animal modal. The imaging studies were performed when tumors reached ~60 mm^3. We intravenously (i.v.) injected HSA-ICG NPs or free ICG (0.5 mg ICG/kg) into mice (n = 3), and acquired FL images on CRI maestro system using a 704 nm excitation wavelength and a 735 nm filter at different time points. The images were unmixed using the Maestro software. Tumour-to-normal tissue ratio (T/N) was determined and was expressed as mean ± SD. All mice were euthanized after the 24 h imaging. Tumours as well as major organs were collected and subjected to *ex vivo* imaging. The FL spectra of HSA-ICG NPs from several locations, including the center of the tumor, tumor margin and normal tissue, were examined by using an NIR FL spectrometer (Inspector Series, DeltaNu). After the spectra were acquired, the integrated signal intensity was calculated. *In vivo* PA imaging was obtained with preclinical photoacoustic computerized tomography scanner (Endra Nexus 128, Ann Arbor, MI).

***In Vivo* Thermal Imaging.** When the tumor size reached ~60 mm^3, HSA-ICG NPs (2 mg ICG/kg) or free ICG (2 mg ICG/kg) was intravenously injected into the tumor-bearing mice. Thermal imaging was recorded by an infrared thermal imaging camera (Ti27, Fluke, USA) when the tumors were exposed to 808 nm laser of power density at 0.8 W/cm^2.

***In Vivo* Synergistic Phototherapy.** For synergistic phototherapy studies, 35 mice bearing 4T1 tumors were randomly divided into seven groups. The treatment scheme is as follows: (1) PBS, no irradiation; (2) HSA-ICG NPs, no irradiation; (3) free ICG (2 mg ICG/kg) plus accurate irradiation (b); (4) HSA-ICG NPs (2 mg ICG/kg) plus interval laser accurate irradiation (5 min interval after each minute of irradiation) (b); (5) HSA-ICG NPs (2 mg ICG/kg) plus part irradiation (a); (6) HSA-ICG NPs (2 mg ICG/kg) plus over irradiation (c); (7) HSA-ICG NPs (2 mg ICG/kg) plus accurate irradiation (b). The photoirradiation was applied 24 h after the injection of HSA-ICG NPs or free ICG (808 nm, 0.8 W/cm^2 for 5 min). The spot of laser beam was adjusted according to the different experiment conditions. The tumor sizes and body weights were inspected every 3 days. The tumor weight was estimated using the formula, tumor volume = length × (width)^2/2,

assuming a tumor density of 1 mg/mL. The volume of tumors was evaluated by normalizing the measured values. After therapy, major organs as well as tumors were collected and sectioned to 8 μm slices for H&E staining.

H&E Staining. H&E staining was performed according to a protocol provided by the vendor (BBC Biochemical). Briefly, 8 μm cryogenic slides were prepared and fixed with 10% formalin for about 30 min at room temperature. After washing with running water for 5 min, the slides were treated with gradient concentrations of alcohol (100, 95, and 70%), each for 20 s. The hematoxylin staining was performed for about 3 min and washed with water for 1 min. The eosin staining was performed for about 1 min. The slides were washed, treated with xylene, and mounted with Canada balsam. The images were acquired on a Nikon Eclipse 90i microscope.

Conflict of Interest: The authors declare no competing financial interest.

Acknowledgment. We are grateful to Dr. Junhui Zhai (United Well Technology Limited (Shanghai)) and Professor Gang Liu (Center for Molecular Imaging and Translational Medicine, Xiamen University) for PA imaging studies. The authors gratefully acknowledge support for this research from the National Natural Science Foundation of China (Grant No. 81301272, 81401521, 81071249, 81171446 and 81371679), Science and Technology Foundation of Guangdong Province of China (Grant No. 2009A030301010) and Shenzhen (JCYJ20130401170306862 and CXZZ20130506140505859), Key Project of Science and Technology of Guangdong (2012B090400043 and 2012B090600036), Nanshan Innovative Technology Program (Grant No. KC2013-JSJS0012A), Guangdong Innovation Team of Low-cost Healthcare, and SIAT Innovation Program for Excellent Young Researchers (201301).

Supporting Information Available: Supplementary methods and results. This material is available free of charge *via* the Internet at http://pubs.acs.org.

REFERENCES AND NOTES

1. Celli, J. P.; Spring, B. Q.; Rizvi, I.; Evans, C. L.; Samkoe, K. S.; Verma, S.; Pogue, B. W.; Hasan, T. Imaging and Photodynamic Therapy: Mechanisms, Monitoring, and Optimization. *Chem. Rev.* **2010**, *110*, 2795–2838.
2. Lal, S.; Clare, S. E.; Halas, N. J. Nanoshell-Enabled Photothermal Cancer Therapy: Impending Clinical Impact. *Acc. Chem. Res.* **2008**, *41*, 1842–1851.
3. Huang, P.; Lin, J.; Wang, X.; Wang, Z.; Zhang, C.; He, M.; Wang, K.; Chen, F.; Li, Z.; Shen, G.; *et al.* Light-Triggered Theranostics Based on Photosensitizer-Conjugated Carbon Dots for Simultaneous Enhanced-Fluorescence Imaging and Photodynamic Therapy. *Adv. Mater.* **2012**, *24*, 5104–1510.
4. Guo, M.; Mao, H.; Li, Y.; Zhu, A.; He, H.; Yang, H.; Wang, Y.; Tian, X.; Ge, C.; Peng, Q.; *et al.* Dual Imaging-Guided Photothermal/Photodynamic Therapy Using Micelles. *Biomaterials* **2014**, *35*, 4656–4666.
5. Chen, R.; Wang, X.; Yao, X.; Zheng, X.; Wang, J.; Jiang, X. Near-IR-Triggered Photothermal/Photodynamic Dual-Modality Therapy System *via* Chitosan Hybrid Nanospheres. *Biomaterials* **2013**, *34*, 8314–8322.
6. Peng, C. L.; Shih, Y. H.; Lee, P. C.; Hsieh, T. M.; Luo, T. Y.; Shieh, M. J. Multimodal Image-Guided Photothermal Therapy Mediated by ^{188}Re-Labeled Micelles Containing a Cyanine-Type Photosensitizer. *ACS Nano* **2011**, *5*, 5594–5607.
7. Lovell, J. F.; Jin, C. S.; Huynh, E.; Jin, H.; Kim, C.; Rubinstein, J. L.; Chan, W. C.; Cao, W.; Wang, L. V.; Zheng, G. Porphysome Nanovesicles Generated by Porphyrin Bilayers for Use as Multimodal Biophotonic Contrast Agents. *Nat. Mater.* **2011**, *10*, 324–332.
8. Cheng, L.; Liu, J.; Gu, X.; Gong, H.; Shi, X.; Liu, T.; Wang, C.; Wang, X.; Liu, G.; Xing, H.; *et al.* PEGylated $WS_{(2)}$ Nanosheets as a Multifunctional Theranostic Agent for *In Vivo* Dual-Modal CT/Photoacoustic Imaging Guided Photothermal Therapy. *Adv. Mater.* **2014**, *26*, 1886–1893.
9. Zhou, M.; Zhang, R.; Huang, M.; Lu, W.; Song, S.; Melancon, M. P.; Tian, M.; Liang, D.; Li, C. A Chelator-Free Multifunctional [^{64}Cu]CuS Nanoparticle Platform for Simultaneous Micro-PET/CT Imaging and Photothermal Ablation Therapy. *J. Am. Chem. Soc.* **2010**, *132*, 15351–15358.
10. Hirsch, L. R.; Stafford, R. J.; Bankson, J. A.; Sershen, S. R.; Rivera, B.; Price, R. E.; Hazle, J. D.; Halas, N. J.; West, J. L. Nanoshell-Mediated Near-Infrared Thermal Therapy of Tumours under Magnetic Resonance Guidance. *Proc. Natl. Acad. Sci. U. S. A.* **2003**, *100*, 13549–13554.
11. Liang, X.; Li, X.; Jing, L.; Yue, X.; Dai, Z. Theranostic Porphyrin Dyad Nanoparticles for Magnetic Resonance Imaging Guided Photodynamic Therapy. *Biomaterials* **2014**, *35*, 6379–6388.
12. Ma, Y.; Tong, S.; Bao, G.; Gao, C.; Dai, Z. Indocyanine Green Loaded SPIO Nanoparticles with Phospholipid-PEG Coating for Dual-Modal Imaging and Photothermal Therapy. *Biomaterials* **2013**, *34*, 7706–7714.
13. Ke, H.; Wang, J.; Dai, Z.; Jin, Y.; Qu, E.; Xing, Z.; Guo, C.; Yue, X.; Liu, J. Gold-Nanoshelled Microcapsules: a Theranostic Agent for Ultrasound Contrast Imaging and Photothermal Therapy. *Angew. Chem., Int. Ed. Engl.* **2011**, *50*, 3017–3021.
14. Sheng, Z.; Song, L.; Zheng, J.; Hu, D.; He, M.; Zheng, M.; Gao, G.; Gong, P.; Zhang, P.; Ma, Y.; *et al.* Protein-Assisted Fabrication of Nano-Reduced Graphene Oxide for Combined *In Vivo* Photoacoustic Imaging and Photothermal Therapy. *Biomaterials* **2013**, *34*, 5236–5243.
15. Liang, C.; Diao, S.; Wang, C.; Gong, H.; Liu, T.; Hong, G.; Shi, X.; Dai, H.; Liu, Z. Tumour Metastasis Inhibition by Imaging-Guided Photothermal Therapy with Single-Walled Carbon Nanotubes. *Adv. Mater.* **2014**, *26*, 5646–5652.
16. Frangioni, J. V. *In Vivo* Near-Infrared Fluorescence Imaging. *Curr. Opin. Chem. Biol.* **2003**, *7*, 626–634.
17. Mohs, A. M.; Mancini, M. C.; Singhal, S.; Provenzale, J. M.; Leyland-Jones, B.; Wang, M. D.; Nie, S. Hand-Held Spectroscopic Device for *In Vivo* and Intraoperative Tumour Detection: Contrast Enhancement, Detection Sensitivity, and Tissue Penetration. *Anal. Chem.* **2010**, *82*, 9058–9065.
18. Wang, L. V.; Hu, S. Photoacoustic Tomography: *In Vivo* Imaging from Organelles to Organs. *Science* **2012**, *335*, 1458–1462.
19. Gao, L.; Fei, J.; Zhao, J.; Li, H.; Cui, Y.; Li, J. Hypocrellin-Loaded Gold Nanocages with High Two-Photon Efficiency for Photothermal/Photodynamic Cancer Therapy *In Vitro*. *ACS Nano* **2012**, *6*, 8030–8040.
20. Jang, B.; Park, J. Y.; Tung, C. H.; Kim, I. H.; Choi, Y. Gold Nanorod-Photosensitizer Complex for Near-Infrared Fluorescence Imaging and Photodynamic/Photothermal Therapy *In Vivo*. *ACS Nano* **2011**, *5*, 1086–1094.
21. Wang, J.; Zhu, G.; You, M.; Song, E.; Shukoor, M. I.; Zhang, K.; Altman, M. B.; Chen, Y.; Zhu, Z.; Huang, C. Z.; *et al.* Assembly of Aptamer Switch Probes and Photosensitizer on Gold Nanorods for Targeted Photothermal and Photodynamic Cancer Therapy. *ACS Nano* **2012**, *6*, 5070–5077.
22. Kalluru, P.; Vankayala, R.; Chiang, C. S.; Hwang, K. C. Photosensitization of Singlet Oxygen and *In Vivo* Photodynamic Therapeutic Effects Mediated by PEGylated $W_{(18)}O_{(49)}$ Nanowires. *Angew. Chem., Int. Ed. Engl.* **2013**, *52*, 12332–12336.
23. Wang, S.; Huang, P.; Nie, L.; Xing, R.; Liu, D.; Wang, Z.; Lin, J.; Chen, S.; Niu, G.; Lu, G.; *et al.* Single Continuous Wave Laser Induced Photodynamic/Plasmonic Photothermal Therapy Using Photosensitizer-Functionalized Gold Nanostars. *Adv. Mater.* **2013**, *25*, 3055–3061.
24. Lin, J.; Wang, S.; Huang, P.; Wang, Z.; Chen, S.; Niu, G.; Li, W.; He, J.; Cui, D.; Lu, G.; *et al.* Photosensitizer-Loaded Gold Vesicles with Strong Plasmonic Coupling Effect for Imaging-Guided Photothermal/Photodynamic Therapy. *ACS Nano* **2013**, *7*, 5320–5329.
25. Sheng, Z.; Hu, D.; Xue, M.; He, M.; Gong, P.; Cai, L. Indocyanine Green Nanoparticles for Theranostic Applications. *Nano-Micro Lett.* **2013**, *5*, 145–150.
26. Yu, J.; Javier, D.; Yaseen, M. A.; Nitin, N.; Richards-Kortum, R.; Anvari, B.; Wong, M. S. Self-Assembly Synthesis, Tumour Cell Targeting, and Photothermal Capabilities of

Antibody-Coated Indocyanine Green Nanocapsules. *J. Am. Chem. Soc.* **2010**, *132*, 1929–1938.
27. Altinoğlu, E. I.; Russin, T. J.; Kaiser, J. M.; Barth, B. M.; Eklund, P. C.; Kester, M.; Adair, J. H. Near-Infrared Emitting Fluorophore-Doped Calcium Phosphate Nanoparticles for *In Vivo* Imaging of Human Breast Cancer. *ACS Nano* **2008**, *2*, 2075–2084.
28. Barth, B. M.; Sharma, R.; Altinoğlu, E. I.; Morgan, T. T.; Shanmugavelandy, S. S.; Kaiser, J. M.; McGovern, C.; Matters, G. L.; Smith, J. P.; Kester, M.; *et al.* Bioconjugation of Calcium Phosphosilicate Composite Nanoparticles for Selective Targeting of Human Breast and Pancreatic Cancers *In Vivo*. *ACS Nano* **2010**, *4*, 1279–1287.
29. Barth, B. M.; Altinoğlu, E.; Shanmugavelandy, S. S.; Kaiser, J. M.; Crespo-Gonzalez, D.; DiVittore, N. A.; McGovern, C.; Goff, T. M.; Keasey, N. R.; Adair, J. H.; *et al.* Targeted Indocyanine-Green-Loaded Calcium Phosphosilicate Nanoparticles for *In Vivo* Photodynamic Therapy of Leukemia. *ACS Nano* **2011**, *5*, 5325–5337.
30. Zheng, C.; Zheng, M.; Gong, P.; Jia, D.; Zhang, P.; Shi, B.; Sheng, Z.; Ma, Y.; Cai, L. Indocyanine Green-Loaded Biodegradable Tumour Targeting Nanoprobes for *In Vitro* and *In Vivo* Imaging. *Biomaterials* **2012**, *33*, 5603–5609.
31. Zheng, M.; Yue, C.; Ma, Y.; Gong, P.; Zhao, P.; Zheng, C.; Sheng, Z.; Zhang, P.; Wang, Z.; Cai, L. Single-Step Assembly of DOX/ICG Loaded Lipid−Polymer Nanoparticles for Highly Effective Chemo-Photothermal Combination Therapy. *ACS Nano* **2013**, *7*, 2056–2067.
32. Zheng, M.; Zhao, P.; Luo, Z.; Gong, P.; Zheng, C.; Zhang, P.; Yue, C.; Gao, D.; Ma, Y.; Cai, L. Robust ICG Theranostic Nanoparticles for Folate Targeted Cancer Imaging and Highly Effective Photothermal Therapy. *ACS Appl. Mater. Interfaces* **2014**, *6*, 6709–6716.
33. Zhao, P.; Zheng, M.; Yue, C.; Luo, Z.; Gong, P.; Gao, G.; Sheng, Z.; Zheng, C.; Cai, L. Improving Drug Accumulation and Photothermal Efficacy in Tumour Depending on Size of ICG Loaded Lipid-Polymer Nanoparticles. *Biomaterials* **2014**, *35*, 6037–6046.
34. Hannah, A.; Luke, G.; Wilson, K.; Homan, K.; Emelianov, S. Indocyanine Green-Loaded Photoacoustic Nanodroplets: Dual Contrast Nanoconstructs for Enhanced Photoacoustic and Ultrasound Imaging. *ACS Nano* **2014**, *8*, 250–259.
35. Wu, L.; Fang, S.; Shi, S.; Deng, J.; Liu, B.; Cai, L. Hybrid Polypeptide Micelles Loading Indocyanine Green for Tumour Imaging and Photothermal Effect Study. *Biomacromolecules* **2013**, *14*, 3027–3033.
36. Liu, P.; Yue, C.; Shi, B.; Gao, G.; Li, M.; Wang, B.; Ma, Y.; Cai, L. Dextran Based Sensitive Theranostic Nanoparticles for Near-Infrared Imaging and Photothermal Therapy *In Vitro*. *Chem. Commun.* **2013**, *49*, 6143–6145.
37. Sharma, P.; Bengtsson, N. E.; Walter, G. A.; Sohn, H. B.; Zhou, G.; Iwakuma, N.; Zeng, H.; Grobmyer, S. R.; Scott, E. W.; Moudgil, B. M. Gadolinium-Doped Silica Nanoparticles Encapsulating Indocyanine Green for Near Infrared and Magnetic Resonance Imaging. *Small* **2012**, *8*, 2856–2868.
38. Moody, E. D.; Viskari, P. J.; Colyer, C. L. Non-Covalent Labeling of Human Serum Albumin with Indocyanine Green: a Study by Capillary Electrophoresis with Diode Laser-Induced Fluorescence Detection. *J. Chromatogr. B: Biomed. Sci. Appl.* **1999**, *729*, 55–64.
39. Elzoghby, A. O.; Samy, W. M.; Elgindy, N. A. Albumin-Based Nanoparticles as Potential Controlled Release Drug Delivery Systems. *J. Controlled Release* **2012**, *157*, 168–182.
40. Elsadek, B.; Kratz, F. Impact of Albumin on Drug Delivery-New Applications on the Horizon. *J. Controlled Release* **2012**, *157*, 4–28.
41. Xu, J.; Wang, J.; Luft, J. C.; Tian, S.; Owens, G. J.; Pandya, A. A.; Berglund, P.; Pohlhaus, P.; Maynor, B. W.; Smith, J.; *et al.* Rendering Protein-Based Particles Transiently Insoluble for Therapeutic Applications. *J. Am. Chem. Soc.* **2012**, *134*, 8774–8777.
42. Riener, C. K.; Kada, G.; Gruber, H. J. Quick Measurement of Protein Sulfhydryls with Ellman's Reagent and with 4,4′-dithiodipyridine. *Anal. Bioanal. Chem.* **2002**, *373*, 266–276.
43. Wu, J.; Song, C.; Jiang, C.; Shen, X.; Qiao, Q.; Hu, Y. Nucleolin Targeting AS1411 Modified Protein Nanoparticle for Antitumour Drugs Delivery. *Mol. Pharmaceutics* **2013**, *10*, 3555–3563.
44. Tian, B.; Wang, C.; Zhang, S.; Feng, L.; Liu, Z. Photothermally Enhanced Photodynamic Therapy Delivered by Nano-Graphene Oxide. *ACS Nano* **2011**, *5*, 7000–7009.
45. Zhen, Z.; Tang, W.; Chuang, Y. J.; Todd, T.; Zhang, W.; Lin, X.; Niu, G.; Liu, G.; Wang, L.; Pan, Z.; *et al.* Tumour Vasculature Targeted Photodynamic Therapy for Enhanced Delivery of Nanoparticles. *ACS Nano* **2014**, *8*, 6004–6013.
46. Dolmans, D. E.; Kadambi, A.; Hill, J. S.; Flores, K. R.; Gerber, J. N.; Walker, J. P.; Borel Rinkes, I. H.; Jain, R. K.; Fukumura, D. Targeting Tumor Vasculature and Cancer Cells in Orthotopic Breast Tumor by Fractionated Photosensitizer Dosing Photodynamic Therapy. *Cancer Res.* **2002**, *62*, 4289–4294.